



HAL
open science

Nitrous acid in marine boundary layer over eastern Bohai Sea, China: Characteristics, sources, and implications

Liang Wen, Tianshu Chen, Penggang Zheng, Lin Wu, Xinfeng Wang,
Abdelwahid S Mellouki, Likun Xue, Wenxing Wang

► To cite this version:

Liang Wen, Tianshu Chen, Penggang Zheng, Lin Wu, Xinfeng Wang, et al.. Nitrous acid in marine boundary layer over eastern Bohai Sea, China: Characteristics, sources, and implications. *Science of the Total Environment*, 2019, 670, pp.282-291. 10.1016/j.scitotenv.2019.03.225 . insu-02078087

HAL Id: insu-02078087

<https://insu.hal.science/insu-02078087v1>

Submitted on 25 Mar 2019

HAL is a multi-disciplinary open access archive for the deposit and dissemination of scientific research documents, whether they are published or not. The documents may come from teaching and research institutions in France or abroad, or from public or private research centers.

L'archive ouverte pluridisciplinaire **HAL**, est destinée au dépôt et à la diffusion de documents scientifiques de niveau recherche, publiés ou non, émanant des établissements d'enseignement et de recherche français ou étrangers, des laboratoires publics ou privés.

1 **Nitrous acid in marine boundary layer over eastern Bohai Sea,**

2 **China: characteristics, sources, and implications**

3
4 Liang Wen^a, Tianshu Chen^a, Penggang Zheng^a, Lin Wu^a, Xinfeng Wang^{a,b*}, Abdelwahid
5 Mellouki^{a,c}, Likun Xue^{a*}, Wenxing Wang^{a*}

6 ^a Environment Research Institute, Shandong University, Qingdao 266237, China

7 ^b State Key Laboratory of Organic Geochemistry, Guangzhou Institute of Geochemistry,
8 Chinese Academy of Sciences, Guangzhou 510640, China

9 ^c ICARE- CNRS/OSUC, 45071 Orléans, France

10 * Corresponding authors. Tel.: +86-532-58631963; fax: +86-532-58631986

11 *E-mail address:* xinfengwang@sdu.edu.cn (X. Wang); xuelikun@sdu.edu.cn (L. Xue);

12 wxwang@sdu.edu.cn (W. WANG).

13
14 **Abstract**

15 Nitrous acid (HONO) serves as a key source of hydroxyl radicals and plays important
16 roles in atmospheric photochemistry. In this study, gaseous HONO and related species
17 and parameters were measured in autumn of 2016 at a marine background site on Tuoji
18 Island in eastern Bohai Sea, China. The HONO concentration in marine boundary layer
19 (MBL) was on average 0.20 ± 0.20 ppbv (average \pm standard deviation) with a maximum
20 hourly value of 1.38 ppbv. It exhibited distinct diurnal variations featuring with elevated
21 concentrations in the late night and frequent concentration peaks in the early afternoon.
22 During nighttime, the HONO was produced at a fast rate with the NO₂-HONO

23 conversion rate ranging from 0.006 to 0.036 h⁻¹. The fast HONO production and the
24 strong dependence of temperature implied the enhancement of nocturnal HONO
25 formation caused by air-sea interactions at high temperature. At daytime, HONO
26 concentration peaks were frequently observed between 13:00-15:00. The observed
27 daytime HONO concentrations were substantially higher than those predicted in the
28 photostationary state in conditions of intensive solar radiation and high temperature.
29 Strong or good correlations between the missing HONO production rate and
30 temperature or photolysis frequency suggest a potential source of HONO from the
31 photochemical conversions of nitrogen-containing compounds in sea microlayer. The
32 source intensity strengthened quickly when the temperature was high. The abnormally
33 high concentrations of daytime HONO contributed a considerable fraction to the
34 primary OH radicals in the MBL.

35

36 **Keywords:** Nitrous acid, marine boundary layer, heterogeneous conversion, daytime
37 HONO, missing HOHO source

38

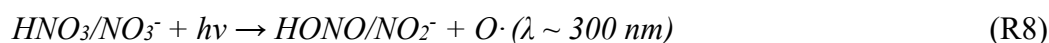
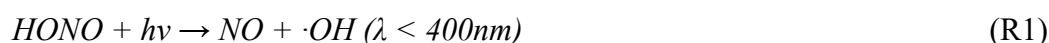
39 **1. Introduction**

40 Nitrous acid (HONO) has been recently confirmed as an important source of
41 hydroxyl radicals (OH radicals) (Alicke et al., 2003; Lee et al., 2013). The photolysis
42 of HONO in near ultraviolet spectral region (R1) directly produces OH radicals which
43 act as the most important atmospheric oxidant in troposphere during daytime (Tang et
44 al., 2015; Wojnárovits and Takács, 2014). Because of the contribution of HONO to OH

45 radicals and the subsequent influence on atmospheric oxidation capacity, the
46 characteristics, sources, and formations, as well as the atmospheric impacts in various
47 environments have attracted close concerns from researchers in the past decade.

48 Gaseous HONO comes from not only primary emissions of anthropogenic and
49 natural sources but also secondary formations involving in NO_x ($\text{NO}_x = \text{NO} + \text{NO}_2$) and
50 other nitrogen-containing compounds. Previous studies have illustrated the high
51 complexity and spatial-temporal dependence of HONO sources in troposphere. In urban
52 and suburban areas, vehicle exhaust is considered to be an important source of HONO
53 with emission factor of HONO/ NO_x ratio ranging from 0.3% to 1.6% (Kurtenbach et
54 al., 2001; Li et al., 2018; Xu et al., 2015). In farmland and forest regions, the HONO
55 can be released from the bacteria in the presence of reactive nitrogen in the soil
56 (Donaldson et al., 2014; Oswald et al., 2013; Su et al., 2011). During daytime, the
57 homogeneous reaction between NO and OH radicals (R2) is known as a major
58 formation pathway of HONO (Alicke et al., 2003). During nighttime, the heterogeneous
59 reactions of NO_2 on wet surfaces of grounds, aerosols, and artificial buildings (R3) have
60 been identified as the main formation pathway (Finlayson-Pitts et al., 2003; Salgado
61 and Rossi, 2002; Spataro et al., 2016; Stutz et al., 2002). The heterogeneous process of
62 NO_2 also produces particulate nitrite which serves as a potential source of HONO in
63 conditions of high temperature, low humidity, and high acidity (R4 and R5) (Costabile
64 et al., 2010; Wang et al., 2015). Recent studies have indicated that in many cases the
65 observed high levels of daytime HONO cannot be explained by the above confirmed
66 HONO sources and some new formation mechanisms have been proposed (Lee et al.,

2016; Legrand et al., 2014; Michoud et al., 2014; Tang et al., 2015; Wang et al., 2017).
 The unexplained daytime HONO is usually attributed to the light-enhanced NO₂
 heterogeneous reactions (R6 and R7) (George et al., 2016; Karamchandani et al., 2015;
 Sörgel et al., 2011). In addition, the daytime HONO can also be produced via the
 photolysis of particulate nitrates or absorbed nitric acid on surfaces of ground or leaves
 (R8) (Kasibhatla et al., 2018; Laufs and Kleffmann, 2016; Oswald et al., 2015; Sörgel
 et al., 2015; Zhou et al., 2011). Overall, the sources and formation mechanisms of
 HONO in different atmospheric environments have not been well recognized and more
 field studies are needed to obtain a comprehensive understanding.



Many field measurements of HONO have been carried out in troposphere within the
 continents (e.g., urban, suburban, rural and remote land) (Costabile et al., 2010; Honrath
 et al., 2002; Su et al., 2008a; Večeřa et al., 2007; Wang et al., 2015; Xu et al., 2015);
 however, only a few studies were conducted in the marine boundary layer (MBL) in
 recent years. Zha et al (2014) measured HONO and related species and parameters at a

81 coastal site along the South China Sea. They found that the nocturnal NO₂-HONO
82 conversion rates in air masses passing over sea surfaces were significantly higher than
83 those over the land and attributed it to air-sea interactions. Wojtal et al (2011) found the
84 temperature dependence of HONO concentrations during nighttime on Saturna Island,
85 adjacent to the Northeast Pacific, and proposed the HONO formation in the sea
86 microlayer (SML). In addition, Meusel et al (2016) observed abnormally high
87 concentrations of daytime HONO with peaks in the late morning under humid
88 conditions on the Cyprus Island in Mediterranean Sea, which was ascribed to the
89 HONO emissions from microbial communities on soil surfaces. Reed et al (2017) and
90 Kasibhatla et al (2018) also found daytime HONO concentration peaks during noontime
91 on Cape Verde Island in tropical North Atlantic, whereas they attributed the daytime
92 peaks mainly to the fast photolysis of particulate nitrates in sea salts. The above field
93 studies have found that the fast HONO formation at nighttime or elevated HONO
94 concentrations during daytime in MBL was linked to some specific local sources.
95 Nevertheless, the unique characteristics of HONO in the MBL and the underlying
96 sources require further confirmation and investigation in other marine regions.

97 In this study, ambient HONO concentrations and related species were measured
98 continuously on an island located in the eastern Bohai Sea, China. We first present the
99 concentrations and various characteristics of HONO and show the obvious nighttime
100 and daytime concentration peaks. Then, the nighttime HONO formation and daytime
101 concentration peaks are explored in details via case analyses and correlation analyses.
102 Finally, the impact of daytime HONO on the primary source of OH radicals is assessed.

103 This study provides some new insights into the characteristics of HONO in a polluted
104 MBL environment in China, and proposes the role of air-sea interaction in the MBL
105 HONO formation and atmospheric photochemistry.

106

107 **2. Experiment and Methods**

108 **2.1 Measurement site**

109 The measurement site was located on a small hill in the north of the Tuoji Island in
110 eastern Bohai Sea, China (38.19°N, 120.74°E, 153 m a.s.l., see Fig. 1). The Tuoji Island
111 was a small rock island (7.1 km²) with a large quantity of rocks and sands on the surface
112 and a few soils in some low areas. The instruments were installed at a temperature-
113 controlled monitoring station on the top floor of a four-story building. The sampling
114 inlets were approximately 1.5 m above the rooftop. The measurement site was
115 surrounded by scattered pine trees and was more than 1000 m far away from the
116 residential villages and fishing piers. Thus, a rare quantity of vehicles and diminutive
117 fishing-boats were the main local anthropogenic emission sources (Wang et al., 2014a;
118 Zhang et al., 2016). To the west of the site, the nearest sea was located and was 160 m
119 far away. The measurement site was more than 10 km away from the nearest major
120 shipping route. The Tuoji Island is far away from the city regions and large industrial
121 sources. Yantai and Dalian, two nearest cities, were situated 40 km to the south and 70
122 km to the north, respectively. The famous Economic Zone of Beijing-Tianjin-Hebei lied
123 190 km to the northwest. Therefore, the measurement site used in this study generally
124 represents the marine atmospheric environment over Bohai Sea. The field

125 measurements were conducted in autumn, from 5th Oct. to 5th Nov., 2016.

126

127 **2.2 Instrument descriptions**

128 A Long Path Absorption Photometer (*LOPAP, Model 03, QUMA, Germany*) was
129 deployed to continuously measure the HONO concentrations with a time resolution of
130 30 s. Ambient gaseous HONO was absorbed simultaneously by sulphanilamide-
131 hydrochloric acid reagent in double tandem glass spiral tubes equipped in an outdoor
132 sampling unit under a constant temperature of 20 °C. More than 99 % of HONO could
133 be collected in the front coil (Kleffmann and P. Wiesen, 2008). The back spiral tube was
134 used to obtain the interference signal caused by other nitrogen compounds in sampling
135 tubes. The absorption solutions through both two spiral tubes were pumped into the
136 instrument and converted to colored azo dye after mixed with N-
137 naphthylethylenediamine-dihydrochloride reagent (Kleffmann et al., 2006). Then, the
138 absorption spectra of these two mixed reagents were measured in two long path
139 absorption tubes with two spectrometers. The raw aqueous concentrations of HONO in
140 the two channels were calculated based on the regular detection of background signal
141 with high-purity nitrogen every 12 hours and the routine calibration by using nitrite
142 standard solution every four days. The HONO concentration in ambient air was finally
143 obtained from the aqueous concentration difference between the two channels and the
144 flow rates of air sample and absorption solution. The detection limit and the uncertainty
145 of the *LOPAP* were 0.2 ppt and 10%, respectively. Refer to Li et al. (2018) for detailed
146 descriptions of the operation and quality assurance and quality control procedures.

147 In addition, relevant pollutants and parameters were measured concurrently with on-
148 line instruments. Specifically, NO was monitored by a chemiluminescence instrument
149 (*Model 42C, Thermo Electron Corporation, USA*). NO₂ was analyzed by a cavity
150 attenuated phase shift spectroscopy (*Model T500U, API, USA*). Ozone was measured
151 by a two-path UV photometric analyzer (*Model 49, Thermo Electron Corporation,*
152 *USA*). CO was detected by a non-dispersive infrared analyzer (*Model 300EU, API,*
153 *USA*). The photolysis frequency of NO₂ represented by J(NO₂) was quantified by a filter
154 radiometer (*Model 2-pi-JNO₂, Meteorologie Consult, Germany*). Meteorological
155 parameters including temperature (T), relative humidity (RH), wind speed (WS) and
156 wind direction (WD) were obtained from an automatic meteorological station (*Model*
157 *PC-4, Jinzhou Sunshine, China*). Detailed information of these instruments can be seen
158 in previous studies (Sun et al., 2016; Wang et al., 2014b; Wang et al., 2012; Xue et al.,
159 2014).

160

161 **2.3 Photostationary state calculation**

162 To assist to understand the observed daytime peaks of HONO, photostationary state
163 (PSS) was assumed during the periods from 9:00 to 15:00 in conditions of strong solar
164 radiation when a balance was achieved quickly between the production and loss due to
165 the fast reaction rates. The PSS HONO concentration (HONO_{PSS}) was calculated via
166 *Eq. (1)* with consideration of only one major source of homogeneous formation (S_{Gas} ,
167 R2) and three loss pathways of photolysis ($L_{Photolysis}$, R1), reaction with OH radical (L_{Gas} ,
168 R9), and dry deposition ($L_{Deposition}$) (Lee et al., 2016). Here, $[NO]$ represents the in-situ

169 measured NO concentration. The values of $J(\text{HONO})$ and $J(\text{O}^1\text{D})$ were estimated based
170 on the relationships between the data of $J(\text{HONO})$ and $J(\text{O}^1\text{D})$ from an Actinic Flux
171 spectrometer (*Model 2-pi-actinic-flux spectrograph, Meteorologie Consult, Germany*)
172 and the data of $J(\text{NO}_2)$ from a filter radiometer in our previous comparative experiment.
173 $[\text{OH}]$ was estimated with an improved empirical formula of Eq. (2) with NO_2 and
174 HONO concentrations together with NO_2 , O_3 , and HONO photolysis frequencies
175 (Alicke et al., 2002). The calculated OH concentration was in the range of 0.1 to 8.6×10^6
176 molecules cm^{-3} , which was a little lower than the measured range during the same
177 daytime period in summer at a suburban site in North China (Lu et al., 2013). The
178 deposition velocity of HONO (v_{HONO}) was set as 0.005 m s^{-1} according to previous
179 studies (Michoud et al., 2014; Stutz et al., 2002). The height of the boundary layer (h)
180 was adopted from the European Centre for Medium-Range Weather Forecasts
181 (<https://www.ecmwf.int/>). The reaction rates ($K_{\text{NO}+\text{OH}}$ and $K_{\text{HONO}+\text{OH}}$) were obtained
182 from the Task Group on Atmospheric Chemical Kinetic Data Evaluation
183 (<http://iupac.pole-ether.fr/index.html>). Note that the heterogeneous NO_2 reactions on
184 aerosol surfaces and the photo-enhanced surface reactions of NO_2 were not considered
185 in the PSS calculation due to the relatively small contributions to the daytime HONO
186 formation. The estimated average HONO formation rate from heterogeneous reactions
187 of NO_2 on aerosol surfaces during daytime was less than 1% compared to the HONO
188 production rate in the PSS period according to the assumptive uptake coefficient of 10^{-6} ,
189 the particulate surface concentration of $2.3 \times 10^{-4} \text{ m}^2 \text{ m}^{-3}$, and the molecular speed of
190 223 m s^{-1} . The photo-enhanced surface reactions of NO_2 contributed approximately

191 1%–10% of the daytime HONO with the assumption that the photo-enhanced NO₂
 192 uptake coefficient rates were one or two orders of magnitude larger than the dark
 193 reactions.



$$[HONO]_{PSS} = \frac{S_{Gas}}{L_{Gas} + L_{Photolysis} + L_{Deposition}} = \frac{[NO] * [OH] * k_{NO+OH}}{[OH] * k_{OH+HONO} + J(HONO) + \frac{v_{HONO}}{h}} \quad Eq. (1)$$

$$[OH] = 4.1 * 10^9 * \frac{J(O^1D)^{0.83} * J(NO_2)^{0.19} * (140 * NO_2 + 1) + HONO * J(HONO)}{0.41 * NO_2^2 + 1.7 * NO_2 + 1 + NO * k_{NO+OH} + HONO * k_{HONO+OH}} \quad Eq. (2)$$

194

195 3. Results and discussion

196 3.1 Concentrations and temporal variations

197 The HONO concentrations in MBL over eastern Bohai Sea in autumn were relatively
 198 high. Table 1 and Fig. 2 show the statistical results and time series of the concentrations
 199 of HONO, related species as well as meteorological parameters during the measurement
 200 period. As shown, the average HONO mixing ratio was 0.20±0.20 ppbv (average ±
 201 standard deviation). The maximum hourly HONO concentration was as high as 1.38
 202 ppbv, appearing at 14:00 local time (LT) on 14th October. The maximum one-minute
 203 value was even higher, reaching 1.90 ppbv. The precursor NO₂ was at a moderately high
 204 level, with an average concentration of 5.3±4.1 ppbv. The average NO and CO
 205 concentrations were 0.5±0.7 and 484±271 ppbv, respectively, indicating a minor
 206 influence from local anthropogenic sources including exhausts of vehicles, boats, and
 207 ships. Ozone, another important source of hydroxyl radicals, appeared in moderate
 208 concentrations with an average value of 40±14 ppbv. When compared to other locations,

209 the HONO concentrations observed over eastern Bohai Sea were lower than those in
210 inland urban areas in Bohai Rim region (Hendrick et al., 2014; Li et al., 2018; Wang et
211 al., 2015), but higher than those in clean marine areas in Mediterranean and tropical
212 North Atlantic (Kasibhatla et al., 2018; Meusel et al., 2016).

213 The HONO concentrations over the eastern Bohai Sea in autumn exhibited large
214 temporal variations. Particularly, the HONO concentrations in the early period (from
215 5th to 21th Oct.) were much higher than those in the later period (from 22th Oct. to 5th
216 Nov.). During the early period, the average HONO concentration was 0.27 ± 0.23 ppbv
217 (also included in Table 1), with a maximum hourly value of 1.38 ppbv. In comparison,
218 during the later period, the average HONO concentration was 0.13 ± 0.11 ppbv and the
219 maximum hourly value was only 0.53 ppbv. In addition, the average HONO/NO_x ratio
220 of 0.057 in the early period was much higher than the ratio of 0.021 in the later period,
221 which means that more HONO was produced in the earlier period than in later period.
222 With examination of related species and meteorological parameters, we find that the
223 concentrations of NO₂, NO, and CO, the winds, and the air masses were comparable in
224 the two periods, while the ambient temperature and photolysis rate of NO₂ in the early
225 period were higher than those in the later period. It indicates that the HONO formation
226 in the early period in conditions of high temperature and intensive solar radiation was
227 possibly quite fast.

228 To further investigate the causes of the HONO variations, we compared the diurnal
229 patterns of HONO and related pollutants and parameters in the two periods (see Fig. 3).
230 Overall, HONO exhibited distinct diurnal variation with two concentration peaks at

231 nighttime and daytime. The nighttime peak appeared in the late night and the daytime
232 peak occurred around 14:00 LT in the early afternoon. During nighttime, the average
233 peak concentration of HONO in the early period was approximately 1.5 times as high
234 as that in the later period (0.37 vs. 0.25 ppbv). Nevertheless, during daytime, the
235 average concentration peak in the early period was up to 3 times as high as that in the
236 later period (0.39 vs. 0.13 ppbv). Moreover, at daytime, the average peak value of
237 HONO/NO_x ratio in the early period was 4.9 time as high as that in the later period
238 (0.127 vs. 0.026). Note that the diurnal patterns and concentrations of NO₂ and NO in
239 the two periods were quite similar, while the temperature and photolysis rate at daytime
240 were significantly higher than those in the later period. The above results suggest that
241 in the early period HONO was produced at very fast rates especially at daytime, which
242 may be linked to the temperature and intensive-sunlight conditions and led to rather
243 high levels of daytime HONO in this period.

244

245 **3.2 Nocturnal HONO formation**

246 In order to obtain a deep understanding of the nighttime HONO formation in MBL,
247 the cases with significant HONO production at nighttime were selected and analyzed
248 in details. The nocturnal cases were identified following the below four criteria: (1)
249 only the data during nighttime (18:00 – 6:00 LT in the next morning) were considered
250 and used; (2) both HONO concentration and HONO/NO₂ ratio increased continuously
251 for more than two hours; (3) the air mass kept unchanged with small wind speed, stable
252 wind direction, and stable CO concentrations; (4) the concentration of the precursor

253 NO₂ had minor change during the selected periods. Finally, eight nocturnal cases (i.e.,
254 6th, 8th, 9th, 13th-14th, 23th, 25th-26th, 30th Oct. and 3rd Nov.) were selected and the NO₂-
255 HONO conversion rate (C_{HONO}) were calculated via Eq. (3) (see Fig. 4 and Table 2).

$$C_{HONO} = \frac{[HONO]_{t_2} - [HONO]_{t_1}}{NO_2 * (t_2 - t_1)} \quad Eq. (3)$$

256 As shown, the continuous increase in HONO concentrations mostly occurred
257 immediately after sunset (i.e., after 18:00) and sometimes started in the late night (after
258 22:00). During the periods for two to five hours, the HONO concentration had increased
259 by 0.13 to 1.07 ppbv and the increase in HONO concentrations exhibited positive
260 correlation with the NO₂ concentration. The nocturnal heterogeneous NO₂-HONO
261 conversion rate ranged from 0.006 to 0.036 h⁻¹, with an average value of 0.018 h⁻¹. The
262 maximum C_{HONO} of 0.036 h⁻¹ appeared in the midnight of 13th Oct., featuring with high
263 temperature (on average 18.8 °C) as well as continuous northerly wind. The NO₂-to-
264 HONO conversion rates at nighttime over the eastern Bohai Sea were obviously higher
265 than the average rate range of 0.003 – 0.010 h⁻¹ at inland sites in the Bohai Rim Region
266 in previous studies (Li et al., 2018; Wang et al., 2017; Wang et al., 2015; Zhang et al.,
267 2019). The facilitated NO₂-to-HONO conversion observed in the MBL in this study
268 was consistent with that found at a coastal site in South China when the air mass came
269 from the marine region and was ascribed to the air-sea interactions (Zha et al., 2014).

270 The nocturnal NO₂-HONO conversion rate in MBL over eastern Bohai Sea varied
271 with atmospheric conditions. Correlation analysis shows a strong positive linear
272 relationship between C_{HONO} and the ambient temperature ($R=0.94$, $p<0.01$). For the
273 selected eight nighttime cases, when the temperature was above 15 °C the C_{HONO} was

274 higher than or equal to 0.02 h^{-1} , while they were all lower than 0.02 h^{-1} when the
275 temperature was below $15 \text{ }^{\circ}\text{C}$ (see Table 2). Nevertheless, C_{HONO} exhibited a moderate
276 correlation with relative humidity ($R=0.57, p<0.01$). The above results indicate that the
277 nocturnal HONO formation from NO_2 over eastern Bohai Sea was enhanced at high
278 temperature. It is consistent with the finding by Wojtal et al. (2011) that the HONO
279 production from NO_2 on seawater surface was largely influenced by the temperature.

280

281 **3.3 Daytime HONO concentration peaks and the missing source**

282 Daytime concentration peaks of HONO were frequently observed in the MBL over
283 eastern Bohai Sea. Figure 5 shows four daytime cases with apparent HONO
284 concentration peaks and stable weather conditions (i.e., sunny, low wind speed, stable
285 wind direction, and stable CO concentration). The daytime concentration peaks of
286 HONO frequently exceeded 0.4 ppbv and the maximum 1-minute value reached 1.90
287 ppbv . The daytime HONO concentration usually started to increase immediately after
288 the solar radiation getting strong and when the temperature was relatively high
289 (approximately above $15 \text{ }^{\circ}\text{C}$). The HONO concentration reached the maximum in the
290 early afternoon (13:00-15:00 LT) after which period the temperature and solar radiation
291 started to drop quickly. Such high concentration peaks of daytime HONO in the
292 presence of intensive solar radiation were rarely observed in other marine regions
293 (Kasibhatla et al., 2018; Meusel et al., 2016). The daytime HONO concentration peaks
294 in the early afternoon observed in this study are different from the daytime peaks
295 appeared in the late morning and noon in the previous studies in other marine areas

296 (Kasibhatla et al., 2018; Meusel et al., 2016). The morning peaks of HONO on the
297 Cyprus Island in Mediterranean Sea were caused by the microbial activities on soil
298 surface after sunrise (Meusel et al., 2016), while the noon peaks on Cape Verde Island
299 in tropical North Atlantic were associated with the photolysis of particulate nitrates in
300 the presence of intense solar radiation (Kasibhatla et al., 2018). The rock dominated
301 surface of the small Tuoji Island together with the unmatched concentration peaks of
302 HONO and NO suggests that microbial activities had little influence on the measured
303 daytime HONO.

304 With the deployment of PSS calculations for the selected four daytime cases, the
305 observed daytime HONO peaks were obviously higher than the PSS prediction, in
306 particular when the ambient temperature was relatively high (also shown in Fig. 5).
307 During 9:00-15:00 on 10th and 14th October, the temperature was always above 15 °C
308 and the observed HONO concentrations were more than two times as high as the PSS
309 calculated values. Whereas, on 6th October and 4th November, the temperature began to
310 exceed 15 °C around the noon and higher HONO observation than PSS prediction only
311 appeared in the early afternoon. In the morning of these two days, the PSS calculated
312 HONO generally matched the observed values. The high daytime concentration peaks
313 of HONO in MBL over eastern Bohai Sea suggest the existences of important missing
314 sources during daytime and the intensity of missing sources was related to the ambient
315 temperature.

316 Correlation analysis using all the data during the PSS periods further confirmed the
317 dependence of the missing HONO source rate ($S(HONO\text{-missing})$, Eq (4)) to the ambient

318 temperature. As shown in Fig. 6, the missing production rate of HONO at daytime
 319 exhibited nearly exponential increase with the temperature ($R=0.69$). When the
 320 temperature was below 15 °C, the missing HONO source rate was small and changeless.
 321 Once the temperature was above 15 °C, the missing production rate sharply increased
 322 with the temperature and was as high as 2 ppbv h⁻¹ when the temperature reached 22
 323 °C. In addition, a rising trend was also found in the missing production rate of HONO
 324 as the photolysis frequency of NO₂ increased (also see Fig. 6). In comparison, no
 325 apparent correlation was found between the values of $S(HONO_{-missing})$ and the humidity,
 326 NO₂ concentrations, or the products of NO₂*J(NO₂). The above results indicate that the
 327 missing sources of daytime HONO were likely light-induced reactions of nitrogen-
 328 containing compounds (e.g., nitrates and nitric acid) on sea surfaces and that the source
 329 intensity was largely influenced by ambient temperature. As reported by Goldstein and
 330 Rabani (2007) and Yang et al (2018) in laboratory studies, the photolysis of dissolved
 331 nitrates produced nitrites at a fast rate which could release gas-phase HONO when the
 332 temperature was relatively high. Therefore, the abnormal daytime concentration peaks
 333 of HONO observed in the MBL over eastern Bohai Sea might be attributed to an
 334 unnoticed source of photolysis of nitrates (or other nitrogen-containing compounds) in
 335 the SML and the subsequent HONO release at relatively high temperature. Future
 336 laboratory or field studies are required to evaluate the accurate production rate of
 337 HONO from photolysis of nitrates in SML on sea surface and the contribution to the
 338 daytime HONO.

$$S(HONO_{-missing}) = ([HONO]_{Meas} - [HONO]_{PSS}) * ([OH] * k_{OH+HONO} + J(HONO) + \frac{V_{HONO}}{h}) \quad Eq. (4)$$

339

340 3.4 Impact of daytime HONO on the primary source of OH radicals

341 The high daytime HONO concentrations observed over the eastern Bohai Sea
342 probably pose a significant impact on the OH radicals through photolysis. Here, we
343 compare the production rate of OH radicals from HONO photolysis and ozone
344 photolysis, which are well known as two major primary sources of OH radicals. The
345 net production rate of OH radicals from HONO photolysis ($P(OH)_{HONO\ net}$) was
346 estimated via Eq. (5) (Su et al., 2008b). The OH production rate from ozone photolysis
347 ($P(OH)_{O_3}$, only from the O¹D branch) was calculated by Eq. (6) (Su et al., 2008b). The
348 involved reaction rate constants were adopted from the Task Group on Atmospheric
349 Chemical Kinetic Data Evaluation of IUPAC (<http://iupac.pole-ether.fr/index.html>).

$$P(OH)_{HONO\ net} = J(HONO) * [HONO] - k_{OH+NO} * [OH] * [NO] - k_{OH+HONO} * [OH] * [HONO] \quad Eq. (5)$$

$$P(OH)_{O_3} = \frac{2 * J(O^1D) * [O_3] * k_{O^1D+H_2O}}{k_{O^1D+H_2O} + k_{O^1D+M}} \quad Eq. (6)$$

350 As shown in Fig. 7, during the periods of 9:00-15:00 in the four daytime cases, the
351 net production rate of OH radicals from HONO photolysis ranged from below zero to
352 several ppbv h⁻¹. The maximum hourly production rate of net OH radicals reached 4.1
353 ppbv h⁻¹, contributing to approximately 49.6 % of the total primary production of OH
354 radicals from both HONO and ozone photolysis. This maximum net production rate and
355 maximum contribution caused by daytime HONO appeared in the early afternoon of
356 14th October, when both HONO concentration and ambient temperature were the
357 highest during the measurement period. Nevertheless, under the conditions of relatively

358 low temperature, the contributions from HONO photolysis were relatively small or
359 even negligible. Overall, the elevated concentrations of daytime HONO over the eastern
360 Bohai Sea at high temperature provided a considerable contribution to the primary
361 source of OH radicals and subsequently to a certain degree enhanced the atmospheric
362 oxidation capacity.

363

364 **4. Conclusions**

365 To understand the characteristics of ambient HONO and its sources and formation
366 mechanisms in a marine region adjacent to the polluted North China, field
367 measurements of HONO and related parameters were conducted from 5th Oct. to 5th
368 Nov. in 2016 at a marine background site on Tuoji Island in the eastern Bohai Sea.
369 Moderately high concentrations of HONO were observed, with the maximum hourly
370 value of 1.38 ppbv. The HONO concentration displayed apparent temporal variation
371 and concentration peaks frequently occurred both in the later night and in the early
372 afternoon. During nighttime, HONO was produced quickly from heterogeneous
373 reactions of NO₂ and the conversion rates were obviously higher than those at inland
374 sites in the Bohai Rim Region. The fast heterogeneous formation of HONO at nighttime
375 was mainly caused by air-sea interactions and was facilitated by the relatively high
376 temperature. During the daytime, the HONO concentration peaks usually appeared in
377 early afternoon in conditions of strong photolysis frequency and high temperature. The
378 photochemical conversions of nitrogen-containing compounds in SML together with
379 the subsequent HONO release under the condition of high temperature were likely to

380 be an important source for the abnormally high daytime HONO. The photolysis of
381 daytime HONO provided a considerable contribution to the primary source of OH
382 radicals and thus should be fully considered in modeling simulations of air quality and
383 atmospheric chemistry.

384

385 **Acknowledgement**

386 This work was supported by the National Natural Science Foundation of China (No.:
387 41505111, 91544213, and 41675118), the National Key Research and Development
388 Program of China (No.: 2016YFC0200500), Marie Skłodowska-Curie actions (H2020-
389 MSCARISE-2015-690958), the Qilu Youth Talent of Shandong University, and the
390 State Key Laboratory of Organic Geochemistry, GIGCAS (Grant No. SKLOG-201616).

391

392 **References**

393 Alicke, B., Geyer, A., Hofzumahaus, A., Holland, F., Konrad, S., Patz, H.W., et al., 2003. OH formation
394 by HONO photolysis during the BERLIOZ experiment. *J. Geophys.Res.* 108.

395 Alicke, B., Platt, U., Stutz, J., 2002. Impact of nitrous acid photolysis on the total hydroxyl radical budget
396 during the Limitation of Oxidant Production/Pianura Padana Produzione di Ozono study in
397 Milan. *J. Geophys.Res.* 107.

398 Costabile, F., Amoroso, A., Wang, F., 2010. Sub- μm particle size distributions in a suburban
399 Mediterranean area. Aerosol populations and their possible relationship with HONO mixing
400 ratios. *Atmos. Environ.* 44, 5258-5268.

401 Donaldson. M.A., Bish, D.L., Raff, J.D., 2014. Soil surface acidity plays a determining role in the

402 atmospheric-terrestrial exchange of nitrous acid. Proc Natl Acad Sci U S A 111, 18472-7.

403 Finlayson-Pitts, B.J., Wingen, L.M., Sumner, A.L., Syomin, D., Ramazan, K.A. 2003. The heterogeneous
404 hydrolysis of NO₂ in laboratory systems and in outdoor and indoor atmospheres: An integrated
405 mechanism. Phys. Chem. Chem. Phys. 5, 223-242.

406 George, C., Beeldens, A., Barmpas, F., Doussin, J-F., Manganelli, G., Herrmann, H., et al., 2016. Impact
407 of photocatalytic remediation of pollutants on urban air quality. Frontiers of Environmental
408 Science & Engineering 10.

409 Goldstein, S., Rabani, J., 2007. Mechanism of Nitrite Formation by Nitrate Photolysis in Aqueous
410 Solutions: The Role of Peroxynitrite, Nitrogen Dioxide, and Hydroxyl Radical. Chem. Soc. 129,
411 10597-10601.

412 Hendrick, F., Müller, J-F., Clémer, K., Wang, P., Mazière, M.D., Fayt, C., et al., 2014. Four years of
413 ground-based MAX-DOAS observations of HONO and NO₂ in the Beijing area. Atmos. Chem.
414 Phys. 14, 765-781.

415 Honrath, R.E., Lu, Y., Peterson, M.C., Dibb, J.E., Arsenault, M.A., Cullen, N.J., et al., 2002. Vertical
416 fluxes of NO_x; HONO, and HNO₃ above the snowpack at Summit, Greenland. Atmos. Environ.
417 36: 2629–2640.

418 Karamchandani, P., Emery, C., Yarwood, G., Lefer, B., Stutz, J., Couzo, E., et al., 2015. Implementation
419 and refinement of a surface model for heterogeneous HONO formation in a 3-D chemical
420 transport model. Atmos. Environ. 112: 356-368.

421 Kasibhatla, P., Sherwen, T., Evans, M.J., Carpenter, L.J., Reed, C., Alexander, B., et al., 2018. Global
422 impact of nitrate photolysis in sea-salt aerosol on NO_x, OH, and O₃ in the marine boundary layer.
423 Atmos. Chem. Phys. 18, 11185–11203.

424 Kleffmann, J., Lörzer, J.C., Wiesen, P., Kern, C., Trick, S., Volkamer, R., et al., 2006. Intercomparison of
425 the DOAS and LOPAP techniques for the detection of nitrous acid (HONO). *Atmos. Environ.*
426 40, 3640-3652.

427 Kleffmann, J., Wiesen, P., 2008, Technical Note: Quantification of interferences of wet chemical HONO
428 LOPAP measurements under simulated polar conditions. *Atmos. Chem. Phys.* 8, 6813–6822.

429 Kurtenbach, R., Becker, K.H., Gomes, J.A.G., Kleffmann, J., Lorzer, J.C., Spittler, M., et al., 2001.
430 Investigations of emissions and heterogeneous formation of HONO in a road traffic tunnel.
431 *Atmos. Environ.* 35, 3385–3394.

432 Laufs, S., Kleffmann, J., 2016. Investigations on HONO formation from photolysis of adsorbed HNO₃
433 on quartz glass surfaces. *Phys. Chem. Chem. Phys.* 18, 9616-9625.

434 Lee, B.H., Wood, C., Herndon, S.C., Lefer, B.L., Luke, W.T., Brune, W.H., et al., 2013. Urban
435 measurements of atmospheric nitrous acid: A caveat on the interpretation of the HONO
436 photostationary state. *J. Geophys. Res. Atmospheres* 118, 12274-12281.

437 Lee, J.D., Whalley, L.K., Heard, D.E., Stone, D., Dunmore, R.E., Hamilton, J.F., et al., 2016. Detailed
438 budget analysis of HONO in central London reveals a missing daytime source. *Atmos. Chem.*
439 *Phys.* 16, 2747-2764.

440 Legrand, M., Preunkert, S., Frey, M., Bartels-Rausch, T., Kukui, A., King, M.D., et al., 2014. Large
441 mixing ratios of atmospheric nitrous acid (HONO) at Concordia (East Antarctic Plateau) in
442 summer: a strong source from surface snow? *Atmos. Chem. Phys.* 14, 9963-9976.

443 Li, D.D., Xue, L.K., Wen, L., Wang, X.F., Chen T.S., Mellouki, A., et al., 2018. Characteristics and
444 sources of nitrous acid in an urban atmosphere of northern China: Results from 1-yr continuous
445 observations. *Atmos. Environ.* 182, 296-306.

446 Lu, K.D., Hofzumahaus, A., Holland, F., Bohn, B., Brauers, T., Fuchs, H., et al., 2013. Missing OH source
447 in a suburban environment near Beijing: observed and modelled OH and HO₂ concentrations in
448 summer 2006. *Atmos. Chem. Phys.*; 13: 1057-1080.

449 Meusel, H., Kuhn, U., Reiffs, A., Mallik, C., Harder, H., Martinez, M., et al., 2016. Daytime formation
450 of nitrous acid at a coastal remote site in Cyprus indicating a common ground source of
451 atmospheric HONO and NO. *Atmos. Chem. Phys.* 16, 14475-14493.

452 Michoud, V., Colomb, A., Borbon, A., Miet, K., Beekmann, M., Camredon, M., et al., 2014. Study of the
453 unknown HONO daytime source at a European suburban site during the MEGAPOLI summer
454 and winter field campaigns. *Atmos. Chem. Phys.* 14, 2805-2822.

455 Oswald, R., Behrendt, T., Ermel, M., Wu, D., Su, H., Cheng, Y., et al., 2013. HONO emissions from soil
456 bacteria as a major source of atmospheric reactive nitrogen. *Science* 341, 1233-1235.

457 Oswald, R., Ermel, M., Hens, K., Novelli, A., Ouwersloot, H.G., Paasonen, P., et al., 2015. A comparison
458 of HONO budgets for two measurement heights at a field station within the boreal forest in
459 Finland. *Atmos. Chem. Phys.* 15, 799-813.

460 Reed, C., Evans, M.J., Crilley, L.R., Bloss, W.J., Sherwen, T., Read, K.A., et al., 2017. Evidence for
461 renoxification in the tropical marine boundary layer. *Atmos. Chem. Phys.* 17, 4081–4092.

462 Sörgel, M., Regelin, E., Bozem, H., Diesch, J.M., Drewnick, F., Fischer, H., et al., 2011. Quantification
463 of the unknown HONO daytime source and its relation to NO₂. *Atmos. Chem. Phys.* 11, 10433-
464 10447.

465 Sörgel, M., Trebs, I., Wu, D., Held, A., 2015. A comparison of measured HONO uptake and release with
466 calculated source strengths in a heterogeneous forest environment. *Atmos. Chem. Phys.* 15,
467 9237-9251.

468 Salgado, M.S., Rossi, M.J., 2002. Flame soot generated under controlled combustion conditions:
469 Heterogeneous reaction of NO₂ on hexane soot. *INT. J. CHEM. KINET.* 34, 620-631.

470 Spataro, F., Ianniello, A., Salvatori, R., Nardino, M., Esposito, G., 2016. Montagnoli M. Sources of
471 atmospheric nitrous acid (HONO) in the European High Arctic. *Rendiconti Lincei* 28, 25-33.

472 Stutz, J., Alicke, Br., Neftel, A., 2002. Nitrous acid formation in the urban atmosphere: Gradient
473 measurements of NO₂ and HONO over grass in Milan, Italy. *J. Geophys.Res.* 107.

474 Su, H., Cheng, Y., Oswald, R., Behrendt, T., Trebs, I., 2011. Meixner FX, et al. Soil Nitrite as a Source
475 of Atmospheric HONO and OH Radicals. *Science* 333, 1616-1618.

476 Su, H., Cheng, Y.F., Cheng, P., Zhang, Y.H., Dong, S., Zeng, L.M., et al., 2008a. Observation of nighttime
477 nitrous acid (HONO) formation at a non-urban site during PRIDE-PRD2004 in China. *Atmos.*
478 *Environ.* 42, 6219-6232.

479 Su, H., Cheng, Y.F., Shao, M., Gao, D.F., Yu, Z.Y., Zeng, L.M., et al., 2008b. Nitrous acid (HONO) and
480 its daytime sources at a rural site during the 2004 PRIDE-PRD experiment in China. *J. Geophys.*
481 *Res.* 113.

482 Sun, L., Xue, L.K., Wang, T., Gao, J., Ding, A.J., Cooper, O.R., et al., 2016. Significant increase of
483 summertime ozone at Mount Tai in Central Eastern China. *Atmos. Chem. Phys.* 16, 10637-
484 10650.

485 Tang, Y., An, J., Wang, F., Li, Y., Qu, Y., Chen, Y., et al., 2015, Impacts of an unknown daytime HONO
486 source on the mixing ratio and budget of HONO, and hydroxyl, hydroperoxyl, and organic
487 peroxy radicals, in the coastal regions of China. *Atmos. Chem. Phys.* 15, 9381-9398.

488 Večeřa, Z., Mikuška, P., Smolík, J., Eleftheriadis, K., Bryant, C., Colbeck, I., et al., 2007. Shipboard
489 Measurements of Nitrogen Dioxide, Nitrous Acid, Nitric Acid and Ozone in the Eastern

490 Mediterranean Sea. *Water, Air, & Soil Pollution: Focus* 8, 117-125.

491 Wang, J.Q., Zhang, X.S., Guo, J., Wang, Z.W., Zhang M.G., 2017. Observation of nitrous acid (HONO)
492 in Beijing, China: Seasonal variation, nocturnal formation and daytime budget. *Sci. Total*
493 *Environ.* 587-588, 350-359.

494 Wang, L.W., Wen L., Xu, C.H., Chen, J.M., Wang X.F., Yang L.X., et al., 2015. HONO and its potential
495 source particulate nitrite at an urban site in North China during the cold season. *Sci. Total*
496 *Environ.* 538, 93-101.

497 Wang, X.P., Chen, Y.J., Tian, C.G., Huang, G.P., Fang, Y., Zhang, F., et al., 2014a. Impact of agricultural
498 waste burning in the Shandong Peninsula on carbonaceous aerosols in the Bohai Rim, China.
499 *Sci. Total Environ.* 481, 311-316.

500 Wang, X., Wang, T., Yan, C., Tham, Y.J., Xue, L., Xu, Z., et al., 2014b. Large daytime signals of N_2O_5
501 and NO_3 inferred at 62 amu in a TD-CIMS: chemical interference or a real atmospheric
502 phenomenon? *Atmos. Measure. Tech.* 7, 1-12.

503 Wang, X.F., Wang, W.X., Yang, L.X., Gao, X.M., Nie, W., Yu, Y.C., et al., 2012. The secondary formation
504 of inorganic aerosols in the droplet mode through heterogeneous aqueous reactions under haze
505 conditions. *Atmos. Environ.* 63, 68-76.

506 Wojnárovits, L., Takács, E., 2014. Rate coefficients of hydroxyl radical reactions with pesticide
507 molecules and related compounds: A review. *Rad. Phy. Chem.* 96, 120-134.

508 Wojtal, P., Halla, J.D., McLaren, R., 2011, Pseudo steady states of HONO measured in the nocturnal
509 marine boundary layer: a conceptual model for HONO formation on aqueous surfaces. *Atmos.*
510 *Chem. Phys.* 11, 3243-3261.

511 Xu, Z., Wang, T., Wu, J.Q., Xue, L.K., Chan, J., Zha, Q.Z., et al., 2015. Nitrous acid (HONO) in a polluted

512 subtropical atmosphere: Seasonal variability, direct vehicle emissions and heterogeneous
513 production at ground surface. *Atmos. Environ.* 106, 100-109.

514 Xue, L.K., Wang, T., Gao, J., Ding, A.J., Zhou, X.H., Blake, D.R., et al., 2014. Ground-level ozone in
515 four Chinese cities: precursors, regional transport and heterogeneous processes. *Atmos. Chem.*
516 *Phys.* 14, 13175-13188.

517 Yang, W., Han, C., Yang, H., Xue, X., 2018. Significant HONO formation by the photolysis of nitrates
518 in the presence of humic acids. *Environ. Pollut.* 243, 679-686.

519 Zha, Q.Z., Xue, L.K., Wang, T., Xu, Z., Yeung, C.P., Louie, P.K.L., et al., 2014. Large conversion rates
520 of NO₂ to HNO₂ observed in air masses from the South China Sea: Evidence of strong
521 production at sea surface? *Geophys. Res. Lett.* 41, 7710-7715.

522 Zhang, J.M., Yang, L.X., Mellouki, A., Wen, L., Yang, Y.M., Gao, Y., et al., 2016. Chemical characteristics
523 and influence of continental outflow on PM_{1.0}, PM_{2.5} and PM₁₀ measured at Tuoji island in the
524 Bohai Sea. *Sci. Total Environ.* 573, 699-706.

525 Zhang, W.Q., Tong, S.R., Ge, M.F., An, J.L., Shi, Z.B., Hou, S.Q. et al., 2019. Variations and sources of
526 nitrous acid (HONO) during a severe pollution episode in Beijing in winter 2016. *Sci. Total*
527 *Environ.* 648, 253-262.

528 Zhou, X.L., Zhang, N., Michaela, T.A., Tang, D., Hou, J., Bertman, S., et al., 2011. Nitric acid photolysis
529 on forest canopy surface as a source for tropospheric nitrous acid. *Nature Geoscience* 4, 440-
530 443.

531

532 **Tables:**

533 **Table 1.** Statistics of ambient concentrations of HONO, other trace gases, and meteorological
534 parameters during the measurement periods (average \pm standard deviation). The T-test was
535 performed for the difference between the two periods.

Species	Full data	5 th – 21 st Oct.	22 nd Oct. – 5 th Nov.	T-test
HONO (ppbv)	0.20 \pm 0.20	0.27 \pm 0.23	0.13 \pm 0.11	$p < 0.01$
NO (ppbv)	0.5 \pm 0.7	0.5 \pm 0.5	0.6 \pm 0.8	$p = 0.32$
NO ₂ (ppbv)	5.3 \pm 4.1	4.8 \pm 3.3	5.9 \pm 4.7	$p < 0.01$
HONO/NO _x	0.040 \pm 0.041	0.057 \pm 0.050	0.021 \pm 0.014	$p < 0.01$
CO (ppbv)	482 \pm 270	478 \pm 239	486 \pm 301	$p = 0.95$
O ₃ (ppbv)	40 \pm 14	45 \pm 15	34 \pm 8	$p < 0.01$
T (°C)	14.2 \pm 3.8	16.8 \pm 1.9	11.3 \pm 3.3	$p < 0.01$
RH (%)	74 \pm 14	76 \pm 12	71 \pm 16	$p < 0.01$
J(NO ₂) (10 ⁻³ s ⁻¹)	1.18 \pm 1.77	1.32 \pm 1.95	1.03 \pm 1.57	$p < 0.05$
WS (m s ⁻¹)	3.7 \pm 2.9	3.4 \pm 2.2	4.1 \pm 3.5	$p < 0.01$

536

537 **Table 2.** The increase and conversion rate of HONO and related pollutant concentrations and
 538 meteorological parameters during the selected periods for the eight nighttime cases.

Date	Duration (h)	Δ HONO (ppbv)	C_{HONO} (h ⁻¹)	Avg. HONO (ppbv)	Avg. NO ₂ (ppbv)	Avg. T (°C)	Avg. RH (%)
6 th Oct.	2.62	0.23	0.020	0.10	4.4	15.8	68
8 th Oct.	2.80	0.15	0.028	0.06	1.9	16.8	79
9 th Oct.	3.18	0.15	0.018	0.09	2.7	14.8	74
13 rd -14 th Oct.	3.33	1.07	0.036	0.41	8.8	18.8	84
23 rd Oct.	4.98	0.25	0.006	0.24	8.9	12.6	71
25 th -26 th Oct.	2.68	0.18	0.016	0.19	4.2	14.1	89
30 th Oct.	3.05	0.13	0.008	0.14	4.8	14.7	54
3 rd Nov.	3.05	0.21	0.010	0.14	7.3	14.1	72

539

540 **Figure captions:**

541 **Fig. 1.** Maps showing the location of the measurement site on Tuoji Island in eastern Bohai Sea,
542 China. (a) The color is coded with the tropospheric NO₂ column density in Oct. 2016
543 (<http://www.temis.nl/index.php>); (b) the color is coded with the topographic height.

544 **Fig. 2.** Temporal variations of the measured HONO, NO_x, CO, O₃, J(NO₂) and meteorological
545 parameters during the measurement period from 5th Oct. to 5th Nov., 2016.

546 **Fig. 3.** Average diurnal patterns of the measured HONO and related parameters for the early period
547 (5th – 21st Oct., the blue line) and the later period (22nd Oct. – 5th Nov., the red line). The shaded
548 areas indicate standard deviations. The shadow areas indicate the nighttime periods (18:00-6:00).

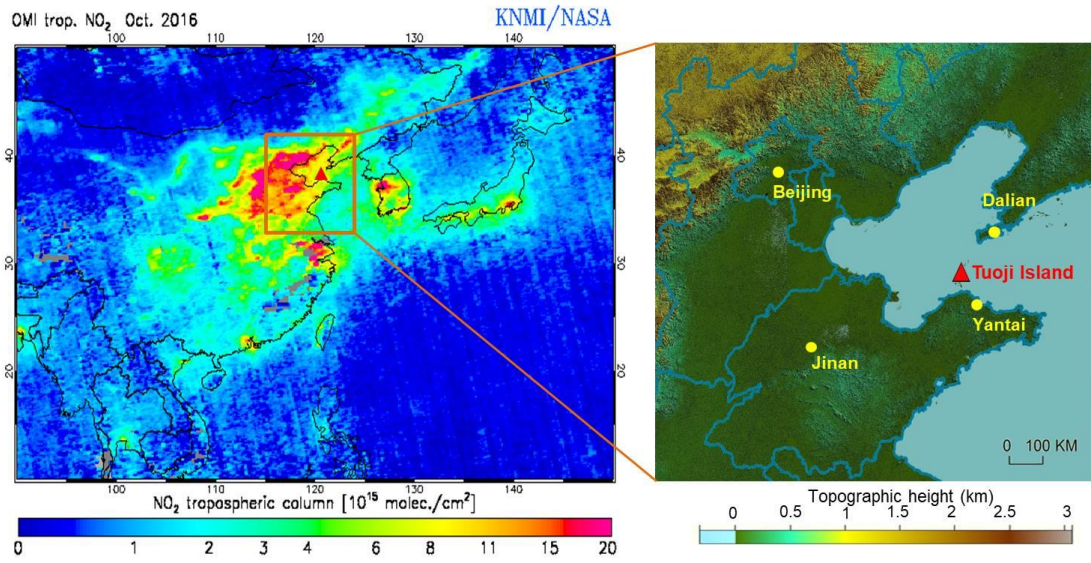
549 **Fig. 4.** Time series of the measured HONO and related parameters for the selected eight nocturnal
550 cases on 6th, 8th, 9th, 13th, 23th, 25th, 30th Oct., and 3rd Nov. The shadow areas indicate the periods
551 with continuous increase in HONO concentrations and HONO/NO₂ ratios.

552 **Fig. 5.** Time series of the measured HONO and related parameters for the selected four daytime
553 cases on 6th, 10th, 14th Oct., and 4th Nov. The shadow areas indicate the PSS periods from 9:00 to
554 15:00.

555 **Fig. 6.** Scatter plots of the missing production rate of HONO (S(HONO_{-missing})) against (a)
556 temperature and (b) J(NO₂) for all hourly data during the PSS periods.

557 **Fig. 7.** The net production rates of OH radicals from photolysis of HONO and ozone as well as the
558 ambient temperature in the four selected daytime cases.

559



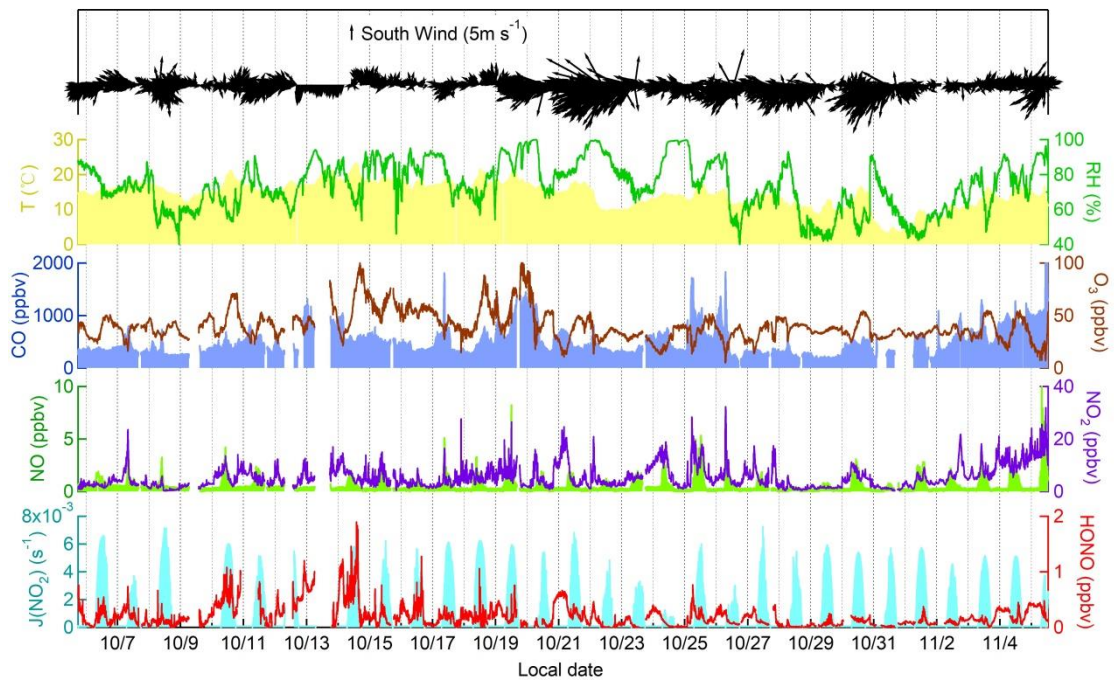
560

561

Fig. 1.

562

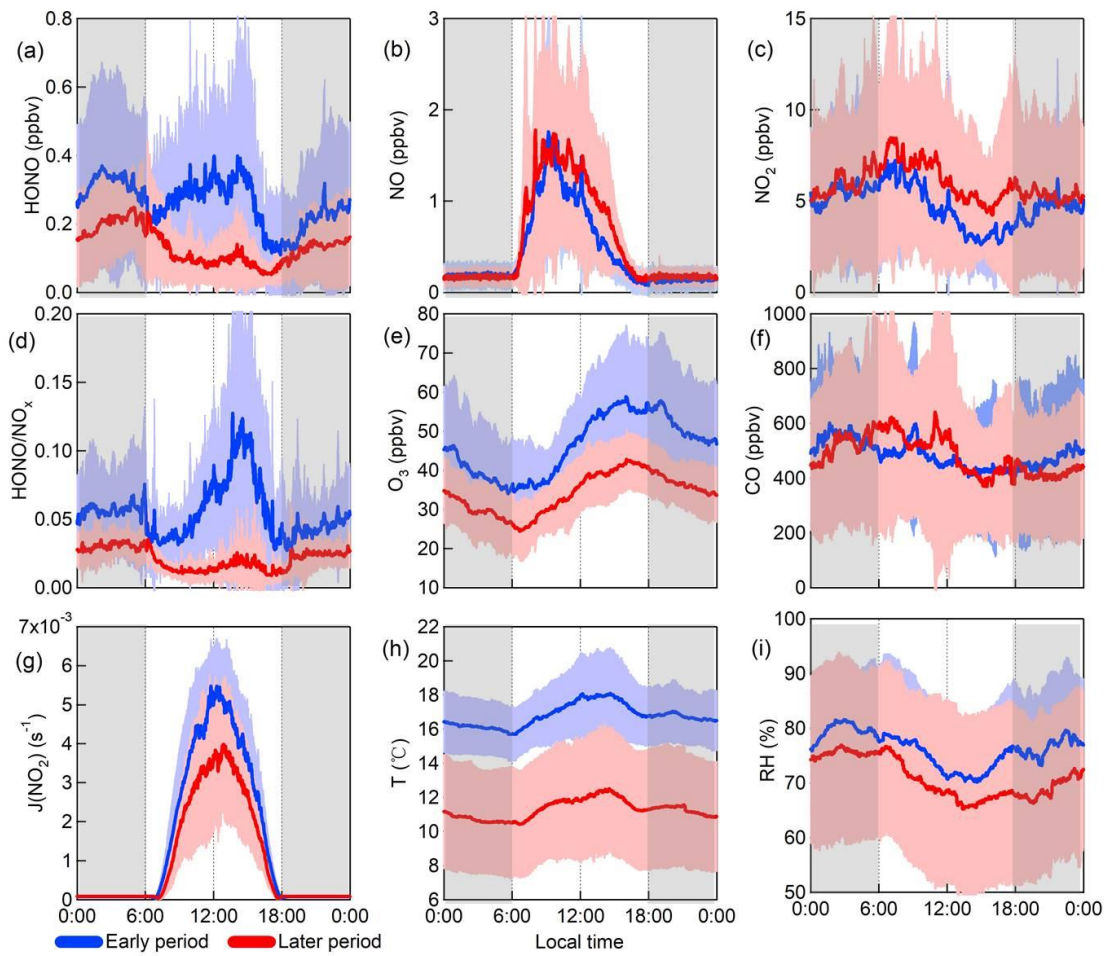
563



564

565

Fig. 2.

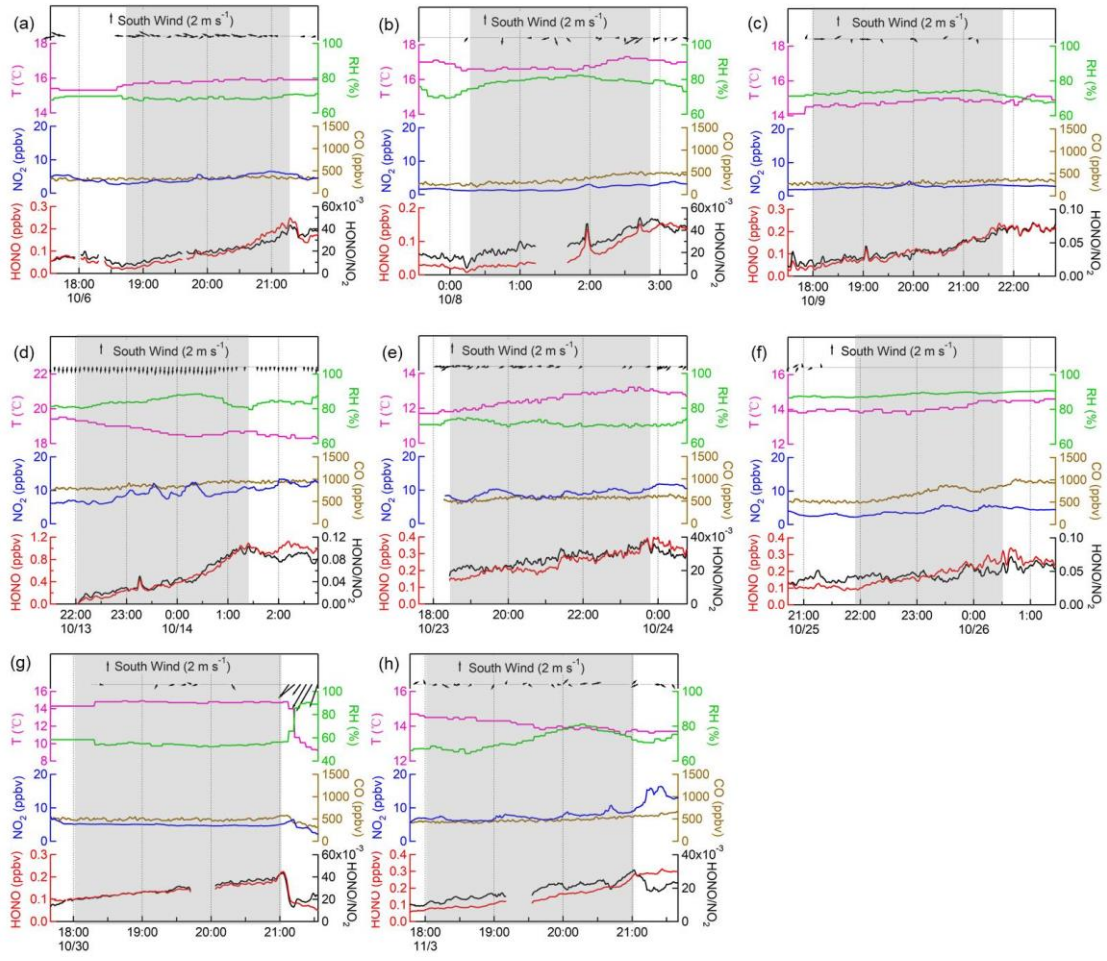


566

567

568

Fig. 3.



569

570

Fig. 4.

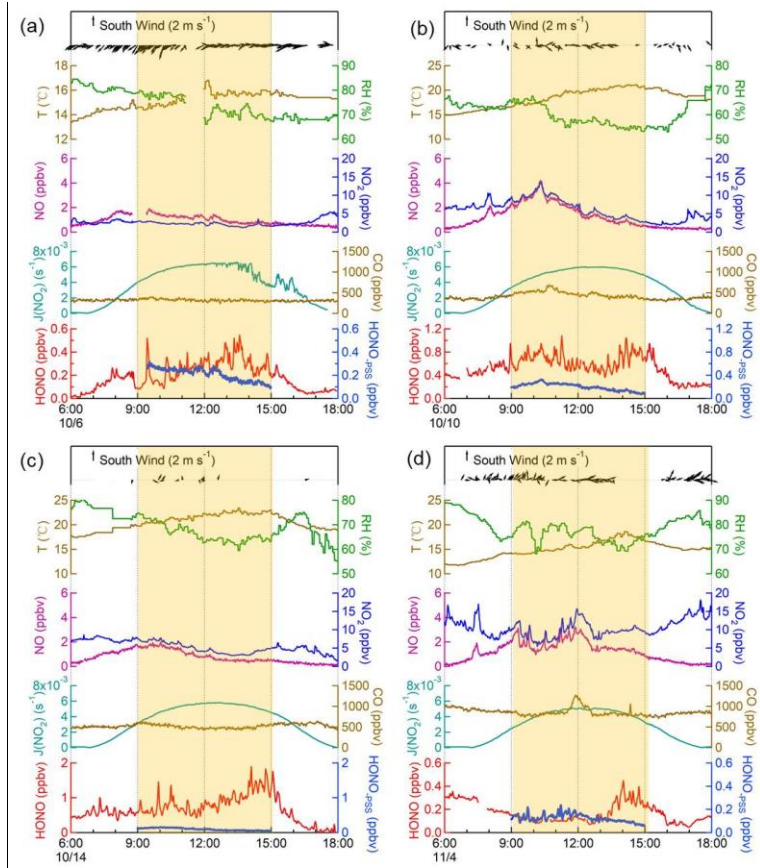


Fig. 5.

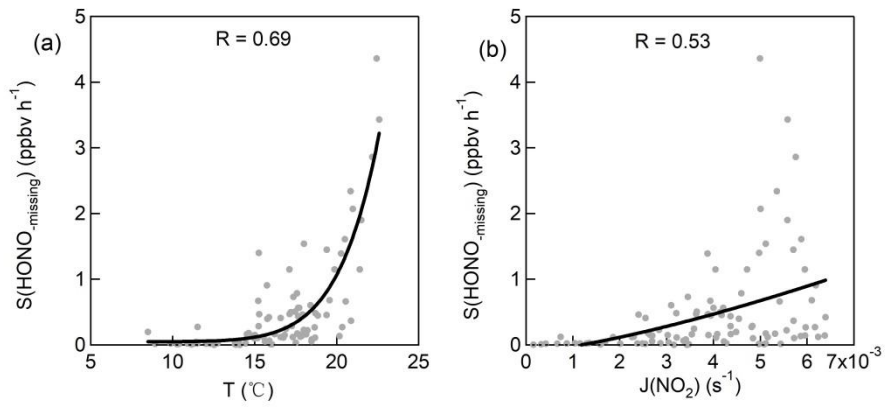


Fig. 6.

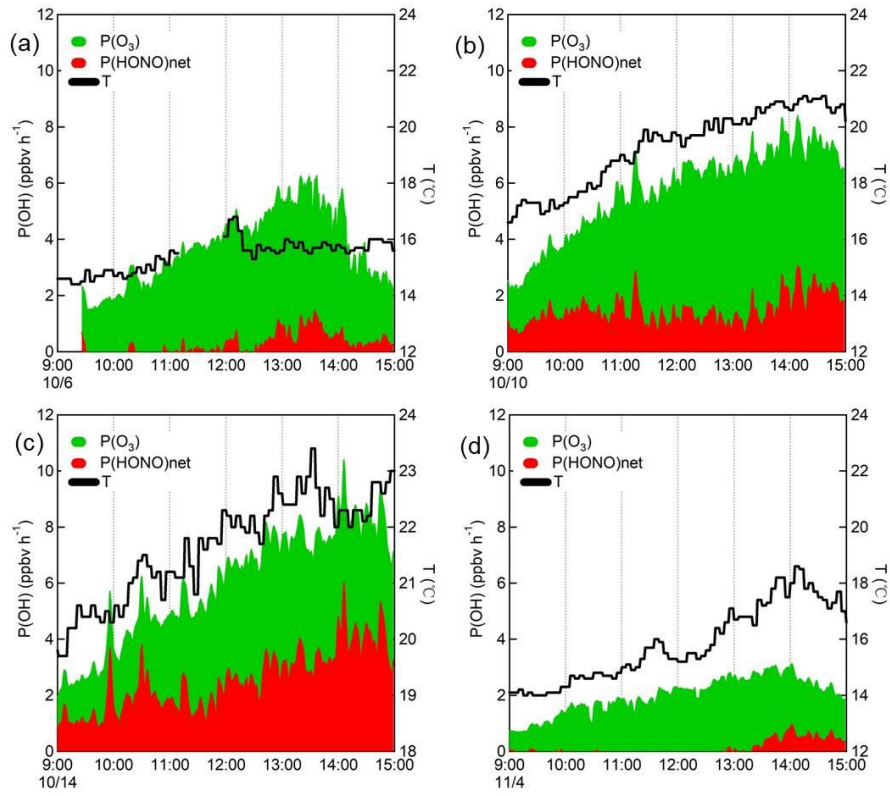
571

572

573

574

575



576

577

Fig. 7.